South African Journal of Botany 168 (2024) 476–487

Contents lists available at ScienceDirect

South African Journal of Botany

journal homepage: www.elsevier.com/locate/sajb

Green synthesis of silver nanoparticles from *Hibiscus tiliaceus* L. Leaves and their applications in dye degradation, antioxidant, antimicrobial, and anticancer activities

Vinay Viswanath Konduri[a], Naveen Kumar Kalagatur[b], Lokanadhan Gunti[c], Usha Kiranmayi Mangamuri[a], Venkateswara Rao Kalagadda[d], Sudhakar Poda[a], Suresh Babu Naidu Krishna[e,f,*]

[a] Department of Biotechnology, Acharya Nagarjuna University, Andhra Pradesh, India
[b] DRDO-BU-Centre for Life Sciences, Coimbatore, Tamil Nadu 641 046, India
[c] Molecular Fungal Genetics and Mycotoxicology Research Unit, Department of Microbiology, Pondicherry University, Puducherry, India
[d] Center for Nanoscience and Technology, Jawaharlal Nehru Technological University, Hyderabad, Telangana 500 085, India
[e] Institute for Water and Wastewater Technology, Durban University of Technology, Durban 4000. South Africa
[f] Department of Biomedical and Clinical Technology, Durban University of Technology, Durban 4000, South Africa

ARTICLE INFO

Article History:
Received 3 August 2023
Revised 6 February 2024
Accepted 18 March 2024
Available online xxx

Edited by Dr B. Ponnusamy

Keywords:
Antioxidant, Antimicrobial
Anticancer
Dye degradation
Green synthesis
Hibiscus tiliaceus L.
Scanning electron microscope

ABSTRACT

The present study reports the green synthesis of silver nanoparticles (AgNPs) from aqueous extract of *Hibiscus tiliaceus* L. leaves and their application in dye degradation, antioxidant, antimicrobial, and anticancer activities. Analysis using Fourier transform infrared (FT-IR) spectroscopy revealed that plant metabolite functional groups had a role in the reduction and stability of AgNPs, and X-ray crystallography (XRD) demonstrated that the AgNPs were in crystal form. The UV–vis spectroscopy, dynamic light scattering (DLS), and zeta potential investigations revealed that the AgNPs were formed with an average size of 88.10 nm in colloidal form and were stable (-49 mV). The field emission scanning electron microscopy (FE-SEM) and high-resolution transmission electron microscopy (HR-TEM) confirmed the shape and size of the AgNPs as spherical with a particle size of 30 - 35 nm, respectively. The AgNPs exhibited potential antioxidant activity by total antioxidant, DPPH, and reducing power assays. The biosynthesized AgNPs displayed a wide range of antibacterial activity on Gram-ve and Gram+ve bacteria by the zone of inhibition assay. AgNPs showed good anticancer activity on MCF-7 cells with an IC_{50} value of 65.83 μg/mL. Furthermore, AgNPs acted as potential catalysts in combination with the reducing agent sodium borohydride ($NaBH_4$) for the degradation of methylene blue (MB), methylene orange (MO), and methylene green (MG) dyes. The degradation efficiency of catalyst AgNPs in the attendance of $NaBH_4$ for 15 min was noted to be 12.8 %, 26.92 %, and 47.56 % for MO, MB, and MG, respectively. The study concluded that green synthesized AgNPs could be highly applicable as an antioxidant, antimicrobial, and anticancer agents in the biomedical field. Furthermore, AgNPs could be helpful in the remediation of dye effluents.

1. Introduction

Research in nanotechnology and nanoscience involves fabricating, describing, investigating, and applying nanomaterials to expand societal needs. This involves manipulating properties, shaping, size, morphology, function, and alignment for various applications. Advances in nanoscience have broadened applications in optics, electronics, mechanics, biomedical sciences, environmental, food, space, drug delivery, energy science, gene delivery, optoelectronic devices, catalysis, and photo-electrochemical devices (Vundela et al., 2022; Suba et al., 2022; Kalagatur et al., 2018; Maheswari et al., 2023).

Silver nanoparticles are an important innovation in nanotechnology due to their high stability and low chemical reactivity. These nanoparticles possess unique physicochemical properties, including electrical conductivity, high thermal behavior, and optical properties. Surface Plasmon Resonance (SPR) makes them suitable for various applications, including textiles, electronics, healthcare medicines, food packaging, and biolabeling. They have potential applications in wound care, antimicrobial dressings, and antitumor agents. AgNPs are also used in consumer products, electronics, and biomedical

* Corresponding author.
E-mail address: sureshk@dut.ac.za (S.B.N. Krishna).

https://doi.org/10.1016/j.sajb.2024.03.035

applications, such as anti-inflammatory, antiviral, and anti-diabetic agents (Raj et al., 2023).

Most cancer deaths are attributed to metastasis. The distinct difficulties in treating metastases arise from their diminutive size, extensive multiplicity, and dispersion across several organ settings. Nanoparticles offer numerous advantages in the diagnosis and treatment of metastatic disease. They may efficiently deliver intricate molecular payloads to key metastatic regions, such as the lungs, liver, and lymph nodes. Additionally, nanoparticles can specifically target particular cell populations inside these organs (Ghatage et al., 2023; Andriani et al., 2020; He et al., 2017; Naraginti and Li, 2017; Mukundan et al., 2015). The discharge of waste effluents from the textile sector is creating significant water contamination, which in turn is leading to a range of health issues in humans. Water contamination is caused by pathogenic microorganisms, discharge of industrial and domestic sewage, as well as runoff from grasslands and agricultural activities. Industrial wastewater is contaminated by organic dyes, which are notable for their harmful characteristics, making them important pollutants. Nanotechnology outperforms conventional techniques in the treatment and remediation of microorganisms and organic dyes. (Ghatage et al., 2023; Naraginti and Li, 2017; Bhakya et al., 2015; Mata et al., 2015).

The synthesis of metal and metal oxide nanoparticles has been reported using physical, chemical, and biological procedures. Physical procedures for nanoparticle synthesis are expensive as high pressure and temperature must be maintained, and it requires continuous consumption of energy, which in turn requires high-end equipment, and there is also a time lag. Chemical synthesis of nanoparticles originates from the production of hazardous by-products that are highlighted as environmental contaminants. Hence, to overcome these problems, biological synthesis of nanoparticles is preferred, as this procedure uses microorganisms and plant materials that are economical, eco-friendly, non-toxic, and abundant, have no by-products, and are easy to handle (Gunti et al., 2022; Lakshmeesha et al., 2019).

Hibiscus tiliaceus, known as beach hibiscus, is an evergreen tree that grows up to 3–10 m in height. It is indigenous to tropical regions, mainly in mangroves of coastal and near coastal areas and subtropical regions like America, Australia, Africa, Asia, and almost all of the Pacific islands. The plant is used as a traditional medicine to treat coughs, fever, dry throat, chest problems, ear infections, diarrhea, dysentery, and typhoid. The extract of *H. tiliaceus* contains various phytochemical compounds that can be used as antioxidant, anti-inflammatory, anthelmintic, and antimicrobial activities. Flowers, roots, leaves, and bark of *H. tiliaceus* are utilized in traditional medicine for various recognized and potential therapeutic characteristics. Also, leaves are used as a wrapping agent around bone fractures, while the fluid from young stems is used to treat skin eruptions as an antibacterial (Surana et al., 2022; Lim et al., 2022; Abdul-Awal et al., 2016).

This study investigated the potential dye degradation, antioxidant, antibacterial, and anticancer competence of *H. tiliaceus* leaf extract-mediated synthesized silver nanoparticles (AgNPs). The biosynthesized AgNPs are characterized by UV-visible spectrophotometer, Fourier-transform infrared spectroscopy (FTIR), dynamic light scattering (DLS), zeta potential, X-ray crystallography (XRD), scanning electron microscopy (SEM), transmission electron microscopy (TEM), and energy-dispersive X-ray spectroscopy (EDX). The antioxidant activity of *H. tiliaceus* leaf extract-mediated synthesized AgNPs was revealed by total antioxidant activity, DPPH free radical scavenging, and reducing power assays. Furthermore, the antibacterial activity of *H. tiliaceus* leaf extract-mediated synthesized AgNPs was performed against both Gram-positive and Gram-negative bacteria by the zone of inhibition assay. Finally, the anticancer activity of *H. tiliaceus* leaf extract-mediated synthesized AgNPs was established on the human breast cancer cell line MCF-7.

2. Materials and methods

2.1. Chemicals and reagents

Silver nitrate, sulphuric acid, sodium hydroxide, l-glutamine, hydrogen peroxide (H_2O_2) solution 30 % (w/w), fetal bovine serum (FBS), Folin-Ciocalteu reagent, sodium carbonate, penicillin, sodium nitrite, streptomycin, Dulbecco's modified Eagle medium (DMEM), deionized water, fetal bovine serum (FBS), phosphate buffer saline of pH 7.4 (PBS), 3-(4,5-dimethylthiazol-2-yl)−2,5-diphenyltetrazolium bromide (MTT), and other chemicals were obtained from Sigma-Aldrich, Bengaluru, India. The live/dead dual staining kit was from Thermo Fisher Scientific, Bengaluru, India.

2.2. Preparation of H. tiliaceus leaf extract

The leaves of *H. tiliaceus* were collected from Guntur, India, and the voucher was recognized and safeguarded in the Department of Biotechnology, Acharya Nagarjuna University, Guntur, India. The leaves were rinsed in deionized water, dried in the shade at room temperature for two weeks, and processed into a fine powder with a blender. The aqueous leaf extract of *H. tiliaceus* was prepared by boiling 6 g of leaf powder in 100 mL of deionized water for 15 min at 80 °C. The aqueous extract was filtered using Whatman No. 1 filter paper and used for further research (Muniyandi et al., 2017).

2.3. Synthesis of AgNPs

A volume of 10 mL of *H. tiliaceus* leaf aqueous extract was added to 90 mL of deionized water, and a concentration of silver nitrate solution was prepared at 1 mM and stirred for 30 min at 300 rpm at 25 ± 2 °C. *H. tiliaceus* leaf extract-mediated synthesis of AgNPs was visually identified by a color shift, which was then confirmed by UV−vis spectroscopy analysis. After UV-visible confirmation, the synthesized AgNPs were centrifuged at 15,000 rpm for 15 min and washed with deionized water thrice, and the pellet obtained was used for further characterization and applications (Naraginti et al., 2016).

2.4. Characterization of AgNPs

The reduction of silver ions in the synthesis of AgNPs was measured in a UV−vis spectrophotometer at wavelengths ranging from 300 to 600 nm (UV−vis double beam spectrophotometer, Systronics 2202, India). The FTIR spectra were considered to confirm the participation of functional biomolecules in reducing silver ions to AgNPs with a wave region of 500–4000 cm^{-1} on a Bruker Alpha II instrument, United States. The XRD pattern of AgNPs was obtained using Bruker D8 Advance, United States, operating a Cu Kα anode (λ = 0.1542 nm) at 40 kV and 30 mA with a step size of 0.05° per step and a dwell time of 12 s per increment at 2θ range from 20 to 80° and 25 °C. The resultant XRD pattern of AgNPs was compared to stoichiometric from the International Centre for Diffraction Data's Powder Diffraction database. The DLS particle size analyzer Horiba SZ 100, United States, was used to determine the size distribution and charge of AgNPs in a colloidal solution. The size and shape of AgNPs were determined by high-resolution transmission electron microscopy, JEM-2100F, JEOL, Japan. The elemental composition of AgNPs was determined from an EDX pattern using high-resolution transmission electron microscopy attached to EDX (JEM-2100F, JEOL, Japan) (Naraginti and Li, 2017).

2.5. Antioxidant activity of AgNPs

2.5.1. Total antioxidant activity

AgNPs were subjected to evaluation of the total antioxidant activities by employing the procedure of Prieto et al. (1999). The AgNPs at five different concentrations of 100–500 μg/mL suspended in 0.05 % DMSO and 0.1 mL aliquots of the sample were mixed with 1 mL of reagent solution, which contains 0.6 M sulphuric acid, 28 mM sodium phosphate, and 4 mM ammonium molybdate. The solution mixture was incubated at 95°C for 90 min and cooled to 25 °C. The absorbance of the solutions was read at 695 nm against the blank solution, which does not contain the test sample using a plate reader (Synergy H1, BioTek, USA). For comparative evaluation, ascorbic acid is used as the standard control. In the total antioxidant assay, the results are taken in ascorbic acid equivalents.

2.5.2. DPPH free radical scavenging activity

The antioxidant property of AgNPs was examined by the DPPH test with a few modifications of the methodology designed by Kalagatur et al. (2020). Briefly, one mL of synthesized AgNPs at different concentrations (100 – 500 μg/mL) suspended in methanol was added to 1 mL of DPPH solution and incubated at 25 ± 2 °C in the dark for 1 hr. The absorbance was recorded at 517 nm λ_{max}. The DPPH activity of the test samples was compared with standard ascorbic acid that was taken as a control. The following formula was used to calculate the DPPH scavenging activity:

DPPH activity = (OD of control - OD of Sample)/ (OD of control) ×100

2.5.3. Reducing power assay

The metal-reducing power of AgNPs was evaluated following the procedure of González-Palma et al. (2016) with slight modifications. Briefly, different concentrations of the AgNPs at 100–500 μg/mL were suspended in 1 mL of phosphate buffer (pH 6.6) at 0.2 M concentration, and 1 mL of potassium hexacyanoferrate (1% w/v). The solution was incubated for 20 min at 50 °C, and the reaction was inhibited by adding 1 mL of trichloroacetic acid (10% w/v). The supernatant was obtained by centrifugation at 3000 rpm for 15 min. Succeeding, supernatant (1.5 mL) was added to 1.5 mL of deionized water and ferric chloride solution (0.1% w/v) and kept undisturbed for about 10 min. Following, absorbance (λ_{max}) readings were measured at 700 nm. The results are expressed in Vitamin E equivalents. Butylated hydroxyl toluene is taken as a standard control.

2.6. Antibacterial activity of AgNPs

The antimicrobial property of the AgNPs was evaluated against two Gram-positive: *Bacillus subtilis* (MTCC 441) and *Staphylococcus aureus* (MTCC 1430), and four Gram-negative: *Escherichia coli* (MTCC 443), *Klebsiella pneumoniae* (MTCC 7162), *Pseudomonas aeruginosa* (MTCC 4996), and *Proteus vulgaris* (MTCC 744), which were obtained from the Microbial Type Culture Collection and Gene Bank (MTCC), Chandigarh, India. A well-diffusion agar plate technique was adopted to study this property (Rosaiah et al., 2022). The bacterial strains were sub-cultured in Lysogeny broth at 37 °C overnight. The colony-forming unit (CFU) was then adjusted to 0.5 McFarland standard by measuring OD at 600 nm using a UV–vis spectrophotometer. The sub-cultured strains were swabbed onto the Lysogeny agar plates, and wells were made using a sterile cork borer. Following, 100 μL of different concentrations of AgNPs (20, 60, 80, and 100 μg/well) were added to wells and incubated at 37°C for overnight observation. The inhibition zone was measured with a measuring scale in mm (ZoneScale, HiMedia, Mumbai, India).

2.7. Anticancer activity of AgNPs

The anticancer activity of AgNPs on MCF-7 (human breast cancer) cells was revealed by MTT and live dead dual staining assays as per the methodology of Gunti et al. (2019). MCF-7 cells were obtained from the National Centre for Cell Science (NCCS), Pune, India, and grown in DMEM with 10 % fetal bovine serum, 1 % of l-glutamine, and 1 % of streptomycin-penicillin at 5 % CO_2 in the humidified atmospheric chamber. Following, confluent cells were trypsinized and used for the study.

In the MTT assay, cells were seeded at 1×10^5 in a 96-well plate and incubated overnight. Following, cells were treated with different concertation of AgNPs for 24 h in DMEM devoid of FBS. The DMEM is used as a control where no nanoparticles are present. Later incubation for 24 hrs, the bright-field inverted microscope was used to observe the morphology of the cells, and MTT assay was performed as per the methodology of Swaminathan et al. (2019). About 20 μL of MTT (5 mg/mL in PBS, pH 7.4) was pipetted in, and 3 hr of incubation was given at 24–25 °C for 3 hrs. Next, 100 μL of DMSO was pipetted into individual wells to liquefy the formazan quartzes. An absorbance λ_{max} at 570 nm was observed in microplate reader equipment (Synergy H1, BioTek, USA). The results were expressed as a percentage of control.

The live/dead cell assay was performed as per the methodology of Kalagatur et al. (2017). Briefly, cells were seeded at 1×10^5 in a 96-well plate and incubated overnight. Following, cells were treated with different concertation of AgNPs for 24 h in DMEM devoid of FBS. The DMEM is used as a control where no nanoparticles are present. Later incubation for 24 hrs, cells were twice-washed in DPBS before being stained for 15 min with 2 μM of calcein AM and 4 μM of ethidium homodimer-1 made in DPBS. Again, cells were washed twice with DPBS; pictures were taken with an inverted fluorescence microscope (EVOS, Life Technologies, United States), employing filters for green fluorescent protein (GFP) and red fluorescent protein (RFP). The live cells stain green, and the dead cells stain red. The live and dead cells were estimated as per the instructions of the kit manufacturer (Thermo Fisher Scientific, USA).

2.8. Catalytic dye degradation activity of AgNPs

Dye degradation studies were done on methylene blue (MB), methyl orange (MO), and malachite green (MG) (Joseph et al., 2015). The dye concentration was 1 mM throughout the experiment, and $NaBH_4$ was prepared at 10 mM. One mL of 10 mM $NaBH_4$ solution was added to 10 mL of 1 mM dye solutions and swirled for 5 min for uniform mixing. To these solution combinations, 1 mL of biosynthesized silver nanoparticles (1 mg/mL) was added, and UV–vis spectrophotometer readings were recorded.

The percentage of dye degradation was calculated as per the following equation.

Colour degradation (%) = $(C_o - C)/C_o \times 100$

2.9. Statistical analysis

The experiments were executed independently in triplicates to avoid an error, and results were expressed as mean ± standard deviation. The data was processed through analysis of variance (ANOVA) and appropriate multiple-range Dunnett's or Tukey's test applied in a completely randomized design to compare the significant differences between the test samples. The 95 % confidence interval ($p \leq 0.05$) was used as the significance criterion. The GraphPad Prism program 8.0 trial version was used for the statistical analysis.

3. Results

3.1. H. tiliaceus *mediated synthesis of AgNPs*

The prepared aqueous extract of *H. tiliaceus* leaf of 10 mL quantity was amalgamated with 90 mL of 1 mM silver nitrate solution (total volume 100 mL). The mixed suspension was subjected to magnetic stirring at 300 rpm for 10 mins, and the formation of AgNPs was visualized in the solution by a change in color to dark brown. To assess the extract solutions, UV–Vis spectroscopy was used to examine the produced Ag nanoparticles.

3.2. *Characterization of AgNPs*

The UV-visible absorbance of the silver colloidal solution is recorded to know the λ_{max} absorption range and to initially confirm the synthesis of AgNPs (Fig. 1A).

The images of FE-SEM of synthesized AgNPs clearly show the shape to be spherical and have a mean size of around 25 nm, as shown in Fig. 1B. The X-ray diffraction report of the synthesized *H. tiliaceus* leaf extract arbitrated AgNPs is shown in Fig. 1C. The diffraction peaks of AgNPs were observed from the range between 10° - 90° d. Five different diffraction peaks can be visualized at 2θ =38.3°, 44.9°, 64.9°, 77.6°, and 81.4°, which represents (111), (200), (220), (311), and (222) reflections affirming the crystallinity of silver nanoparticle. The pattern was found with JCPDS file no: 04–0783. The visualized unassigned peaks are considered to be the peaks of the bio-molecules existing in the leaf extract that act as the capping and stabilizing agents (Bar et al., 2009; Mukundan et al., 2015).

FTIR spectroscopy analysis studies the biomolecules existing in the aqueous extract of *H. tiliaceus* leaf that was accountable for the reduction, and they act as capping agents to provide stability of the synthesized AgNPs (Fig. 1D). The infra-red spectrum of the AgNPs displayed an intense vibrational peak at 3444.77 cm^{-1}, 2920 cm^{-1}, 1725.65 cm^{-1}, 1631.27 cm^{-1}, 1384.17 cm^{-1}, 1124.44 cm^{-1}, 1113.68 cm^{-1}, and 617.03 cm^{-1}. The strong absorption band at 3444.77 cm^{-1} visualized specifies the existence of free OH phenols and alcohol compounds. The absorbance peak at 2920 cm^{-1} signifies the occurrence of the OH group of R-COOH and the C-H stretching of alkene compounds.

The Zeta potential analysis documents the stability of the nanoparticles synthesized. The zeta potential of produced AgNPs was documented as −49 mV, which implies that the AgNPs are more stable (Fig. 1E). The results of the DLS showed the mean size of AgNPs to be 88.10 nm (Fig. 1F). The polydispersity index (PDI) is used to estimate the mean uniformity distribution of the nanoparticle in the solution. If the PDI is less than 0.1, the nanoparticles are stated as monodisperse. HR-TEM images of the AgNPs can be seen in Fig. 1G, which reports the shape of the AgNPs, which is spherical and well-distributed without agglomeration.

3.3. *Antioxidant activity of AgNPs*

The antioxidant potency of *H. tiliaceus* leaf extract mediated synthesized AgNPs synthesized AgNPs was assessed by different assays such as total antioxidant, DPPH free radical, and reducing power analysis (Fig. 2). The total antioxidant activity of AgNPs was shown in Fig. 2A. The total antioxidant activity obtained for AgNPs was compared with ascorbic acid, which was the standard control. The results showed that increased AgNPs concentration increased the total antioxidant activity (dose-dependent). The results showed a better antioxidant activity at a concentration of 500 μg/mL of AgNPs, which was found equivalent to 64.81 ± 3.94 μg of ascorbic acid.

The DPPH radical scavenging property is a commonly used procedure to assess the antioxidant properties of different samples. Due to DPPH's spare electron decolonization over the molecules, it acts as a free radical. A color change in the solution from violet to pale yellow notes the movement of H^+ to the DPPH. The DPPH free radical scavenging property showed a constant reduction in absorbance λ_{max} at 517 nm. Fig. 2B shows the graph of DPPH free radical inhibition (%) versus different concentrations of AgNPs. The DPPH free radical scavenging property of AgNPs enhanced as the concentration of the AgNPs increased (dose-dependent). The results showed a 92.18 ± 2.71 % inhibition of DPPH radicals at 500 μg/mL.

Fig. 2C displays the reducing property of AgNPs at different concentrations ranging between 100 and 500 μg/mL. The reducing power property of AgNPs were of in the order 100 < 200 < 300 < 400 < 500 μg/mL (dose-dependent). The results showed a better antioxidant activity at a concentration of 500 μg/mL of AgNPs, which was found to be equivalent to 53.29 ± 1.88 μg of ascorbic vitamin E equivalent.

3.4. *Antibacterial activity of AgNPs*

H. tiliaceus leaf extract mediated synthesized AgNPs) displayed antibacterial activity against six bacterial strains, two Gram-positive: *B. subtilis* (MTCC 441) and *S. aureus* (MTCC: 1430), and four Gram-negative: *E. coli* (MTCC 443), *K. pneumoniae* (MTCC 7162), *P. aeruginosa* (MTCC 4996), and *P. vulgaris* (MTCC 744). A potent antibacterial activity of AgNPs was documented against Gram-positive as well as Gram-negative bacteria. The zone of inhibition is calculated in millimeters (mm) and is shown in Table 1. The maximum zone of inhibition was recorded against *E. coli* (MTCC 443) and *P. vulgaris* (MTCC 744) (Fig. 3 and Table 1). This can be accredited to the instigation of $silver^+$ ions from silver nanoparticles. The bacteria cell membrane comprises phospholipid bilayers and protein biomolecules, and the phospholipid bilayer is negatively charged. Therefore, positively charged silver ions combine with negatively charged bacteria cell bilayer, leading to physical changes in the cell wall of the bacterial species, causing severe damage. Moreover, the silver ions might also be involved in the sulfhydryl group (-SH) of the bacterial enzyme, causing damage to the enzymes (Hovhannisyan et al., 2022; Scandorieiro et al., 2022).

3.5. *Anticancer efficacy of AgNPs against MCF-7 cells*

The anticancer activity of green synthesized AgNPs was studied against human breast cancer cell line MCF-7 with a dose-dependent variation of AgNPs by MTT assay. From Fig. 4A, it is evident that an initial concentration of as low as 20 μg/mL had triggered cytotoxicity against the MCF-7 cell line with 12.19 % of cell death, and at 100 μg/mL, the cell death reached 78.95 %. The IC50 value (concentration required to inhibit 50 % of cell viability) of AgNPs was calculated to be 65.83 μg/mL against MCF-7 cells. As seen in Fig. 4B, MCF-7 cells indicated morphological variations demonstrating apoptosis when treated with 50 and 85 μg/mL of AgNPs, suggesting these AgNPs exhibit excellent anticancer properties. Furthermore, the anticancer effect of AgNPs was visually revealed by live/dead dual staining assay, comprising calcein AM and ethidium homodimer 1. Cells treated with 50 and 85 μg/mL of AgNPs showed red-colored cells (dead) compared to control cells and indicated that AgNPs had affected the viability of the MCF-7 cancer cells and have potential anticancer efficacy (Fig. 4B).

3.6. *Remediation of dyes using AgNPs*

Fig. 5 shows the UV-visible absorption spectra and plot of ln (At/A0) versus time for methylene blue, orange, and malachite green dye degradation in $NaBH_4$. Furthermore, we have observed that $NaBH_4$ and AgNPs improved the degradation of methylene blue, methylene orange, and malachite green dyes, as shown in Fig. 6.

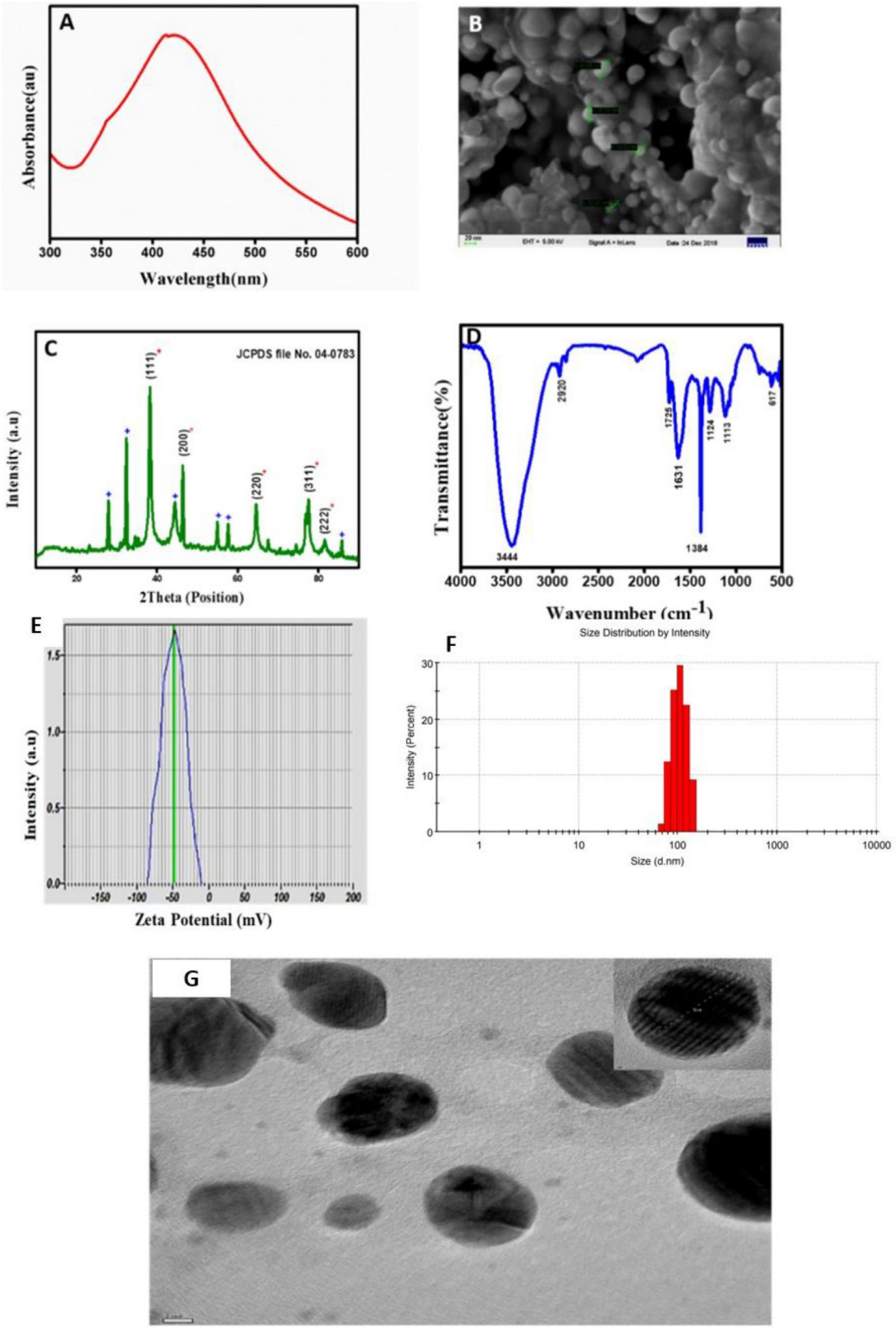

Fig. 1. Characterization of *H. tiliaceus* mediated synthesized silver nanoparticles (AgNPs). (A) UV-visible absorption spectra. (B) FE-SEM images. (C) X-ray Diffraction pattern. (D) FTIR spectra. (E) Zeta potential. (F) DLS pattern. (G) HR-TEM image.

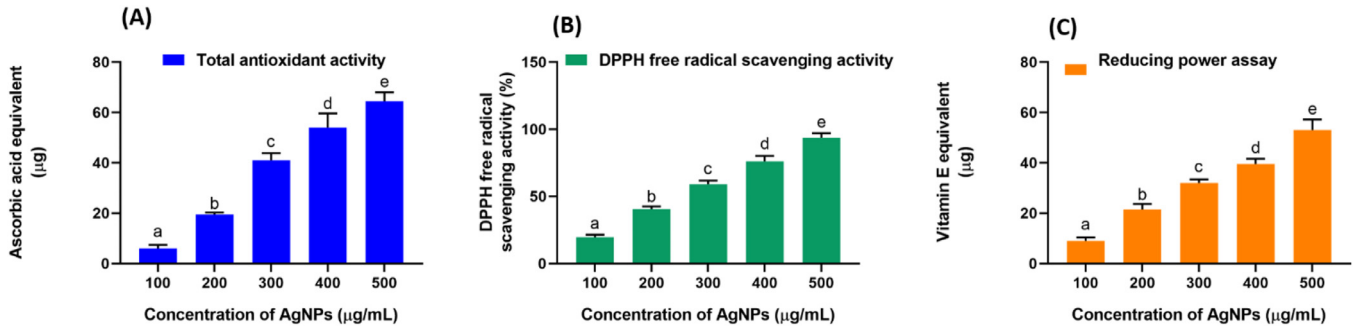

Fig. 2. Dose-dependent antioxidant potential of *H. tiliaceus* mediated silver nanoparticles (AgNPs). (A) Total antioxidant activity. (B) DPPH free radical scavenging activity. (C) Reducing power assay. Using Tukey's test, the statistical significance between the test samples was established; a p-value ≤ 0.05 was considered significant. Different alphabet bar graphs indicate the statistical significance among test samples in the specific study group.

Table 1
Zone of inhibition (mm) for anti-bacterial activity of silver nanoparticles.

Bacterial strain	Zone of inhibition (mm)			
	Silver nanoparticles concentrations (μg/well)			
	20 (μg/well)	60 (μg/well)	80 (μg/well)	100 (μg/well)
Bacillus subtilis (MTCC: 441)	5.18 ± 0.09	7.09 ± 0.08	9.12 ± 0.25	10.91 ± 0.29
Staphylococcus aureus (MTCC: 1430)	3.22 ± 0.03	5.32 ± 0.12	8.27 ± 0.17	10.88 ± 0.24
E. coli (MTCC: 443)	2.15 ± 0.04	4.81 ± 0.09	8.41 ± 0.14	12.31 ± 0.31
Klebsiella pneumoniae (MTCC: 7162)	2.81 ± 0.03	4.39 ± 0.08	5.59 ± 0.11	10.70 ± 0.22
Pseudomonas aeruginosa (MTCC: 4996)	2.57 ± 0.03	5.63 ± 0.09	6.01 ± 0.18	10.47 ± 0.18
Proteus vulgaris (MTCC: 744)	2.70 ± 0.04	4.88 ± 0.08	8.64 ± 0.27	11.94 ± 0.19

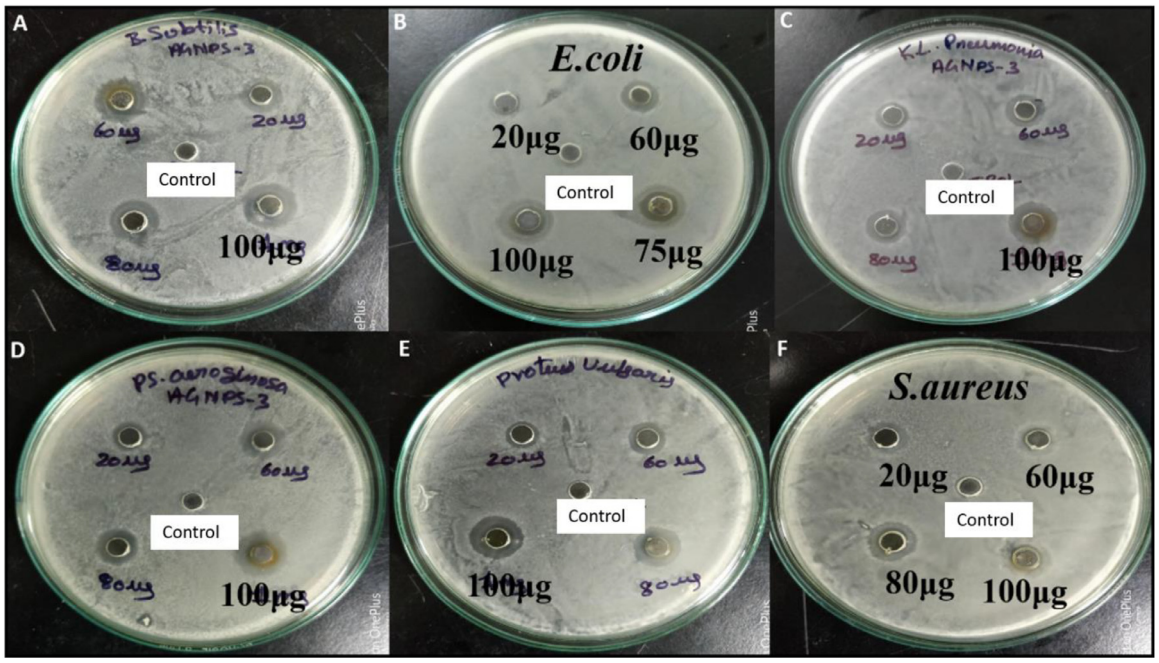

Fig. 3. Antibacterial activity of *H. tiliaceus* mediated synthesized silver nanoparticles (AgNPs) against selected microbes by zone of inhibition assay.

At first, only $NaBH_4$ was introduced, but the dyes could not be completely removed due to high bond dissociation energy (BDE) and limited electron transfer (Fig. 5A). As an intermediary in the reaction between MB dye and NaBH4 ions, silver nanocatalyst lowers the BDE, improving electron transport. Fig. 6A demonstrates that AgNPs increased NaBH4′s MB reduction rate and that the dye degraded in 35 min. A linear association between ln (At/A0) and reduction time in min was found in Fig. 6B using the pseudo-first-order kinetic model for MB degradation. The graph slope revealed the rate constant (k) as 0.101 min^{-1}. The rate constant and regression values are shown in Table 2.

No color change was seen when $NaBH_4$ was added to the dye solution to degrade MO. Fig. 5C shows that increased BDE extended MO reduction with NaBH4. When AgNPs were introduced to dye and NaBH4, the reaction mixture quickly decolorized, showing their catalytic impact in MO degradation. The UV–Vis absorption spectra peaks of MO dye decreasing steadily owing to degradation by $NaBH_4$ in the presence of AgNPs as a nano-catalyst are shown in Fig. 6C. MO

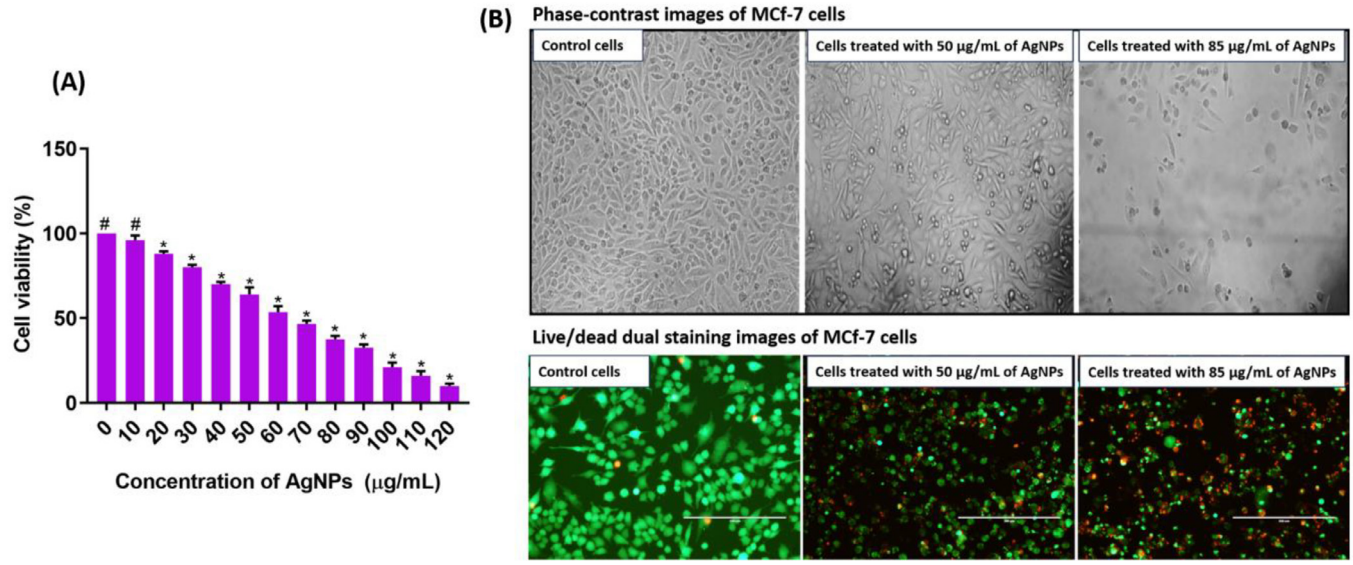

Fig. 4. (A) Dose-dependent anticancer effect of anticancer effect of *H. tiliaceus* mediated silver nanoparticles (AgNPs) determined by MTT and live/dead dual staining assays. The statistical analysis between control and test samples was calculated by Dunnett's test and significance was considered at $p \leq 0.05$. There is no discernible difference between the test sample and the control sample, as denoted by the asterisk (#). The significance of the test sample in comparison to the control is indicated by the asterisk (*). (B) Phase-contrast and live/dead dual staining microscopic images of MCF-7 cells showing anticancer effect of AgNPs. In live/dead dual staining, green and red color depicts the live and dead cells, respectively.

deteriorated in 45 min with AgNP nanocatalysts. Dye reduction followed by pseudo-first-order kinetics to MO dye is shown in Fig. 6D by the linear correlation between ln (At/A0) and reduction time in min. The graph slope gives the rate constant as 0.117 min^{-1}.

Malachite green ($C_{23}H_{25}ClN_2$) is a triarylmethane color used in dyestuff and pigment industries. Fig. 5E indicates that $NaBH_4$ did not improve MG decomposition. AgNPs degrade dye in 10 min, as seen in Fig. 6E. AgNPs catalyse MG degradation by decreasing absorbance. The linear correlation between ln (At/A0) and degradation time in Fig. 6F indicates pseudo-first-order MG dynamics. The graph slope (Table 2) yields 0.176 min-1 for the rate constant (k).

We found an induction period (IP) for all three degradation processes (Fig. 7). After IP, dye concentrations decreased steadily, as demonstrated in Fig. 7D, which shows smooth graphs of ln [A] vs time obtained for MB, MO, and MG degradation using AgNPs as nanocatalyst and $NaBH_4$ as reducing agent at 30 °C. The dye degradation efficiency C/Co in Fig. 7A–C illustrates that the dye degrades over time. Fig. 8 shows the graph of degradation percentage vs. time, which matches calculated values for dye degradation using silver nanoparticles as nanocatalyst and $NaBH_4$ as reducing agent. The dyes' degradation percentage was calculated at 15 min to measure their stability.

4. Discussion

The scientific community is most interested in synthesizing AgNPs because of their potential use in catalysis, optronics, sensing, and medicines. Multiple plants and weeds have emerged as potential reducing agents for silver nitrate during the production of AgNPs. Plants adapt to their environments by producing organic metabolites with different structures. Therefore, there is notable diversity in the properties of AgNPs produced biologically (Ghatage et al., 2023; Khane et al., 2022).

In this study, the development of AgNPs is reflected by a significant absorption maximum at 420 nm, which indicates the reduction of Ag^+ ions by *H. tiliaceus* leaf extract. Peak/absorption maxima reveal exciting details about the nanoparticles' form after synthesis. The typical absorbance peak of synthesized AgNPs is visualized by the color change from pale yellow to dark brick color, and λ_{max} absorbance between 400 - 450 nm range was documented that shows AgNPs absorbing visible range (spectrum) and exhibiting SPR (Bhakya et al., 2015). The location and status of the surface plasmon resonance (SPR) peak depend on the shape, dimensions, and dielectric constant of the sample solution (Mata et al., 2015). Smaller NPs have absorption maxima at longer wavelengths, whereas larger NPs have absorption maxima at shorter wavelengths. The present study's absorption peak at a substantially shorter wavelength (420 nm) suggests the production of nanoparticles with smaller in size.

In the present study, SEM images reveal the presence of bigger particles of AgNPs, which can be attributed to the aggregation of nanoparticles. This aggregation is likely caused by the evaporation of the solvent during the sample preparation process. This factor may have played a role in the observed variability in particle size. The as-synthesized AgNPs were crystalline in nature. Similar findings were made by Jeeva et al. (2014), who discovered crystalline peaks (32.28°, 46.28°, 54.83°, 67.47°, and 76.69°) that were also readily apparent in several other papers whose XRD patterns included the pertinent 2° range. The presence of phytochemical substances in the *H. tiliaceus* leaf extracts is responsible for the observed appearances of these peaks. The enhanced levels of planes show the presence of silver as a significant component in biosynthesis. The result obtained from FTIR supports the existence of O-H and N-H, the key components of the flavonoids, phenols, and alkaloids in the *H. tiliaceus* aqueous leaf extract, acted as the main reducing and capping agents for the AgNPs synthesis. The protein molecules that might be present on the surface of the AgNPs act as surfactants to prevent agglomeration, thereby increasing the stability of AgNPs (Ajitha et al., 2014; Narayanan and Sakthivel, 2011). The vibrational peak visualized at 1631.27 cm^{-1} indicates the presence of the amide I molecule. The vibrational band at 1384.17 cm^{-1} specifies the C-C stretch of the aromatic molecules. The vibrational band at 1124.44 cm^{-1} and 1113.68 cm^{-1} documents the C-O bending of alkene, carboxylic acid, alcohol, ester, and ether. The vibrational peak at 617.03 cm^{-1} witnessed the aromatic C-H bending. In addition, it is observed from the obtained results that the -OH, C=O, and C-N-related functional groups might have been involved in the production of AgNPs. The results visualized support the earlier cited research reports that document that the extract of the *H. tiliaceus* leaf contains the bio-molecules accountable for the synthesis of AgNPs (Ajitha et al., 2014).

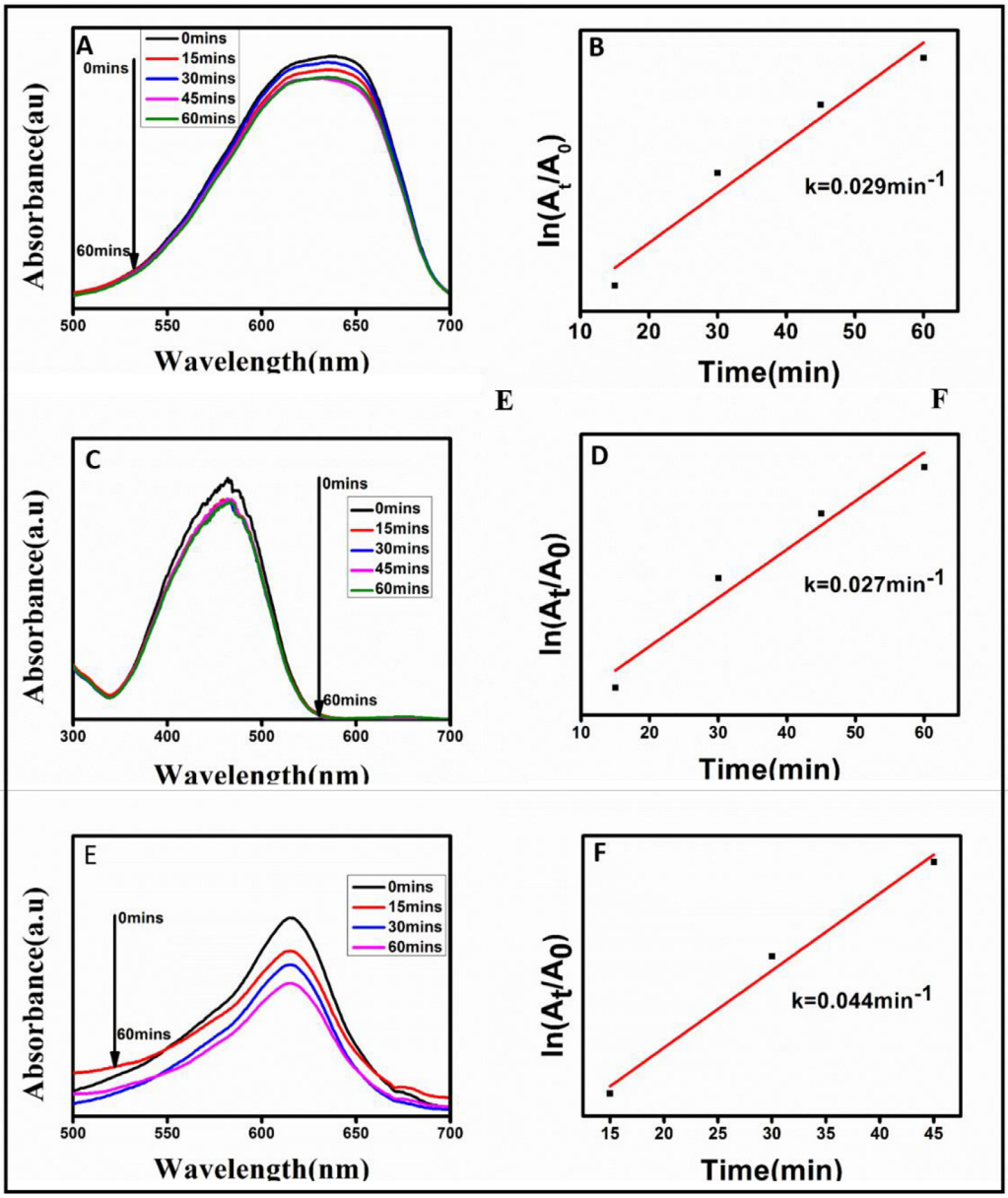

Fig. 5. UV-visible absorption spectra of degradation of dyes [(A) methylene blue, (C) methylene orange, and (E) malachite green] in the presence of $NaBH_4$. The plot of $\ln(A_t/A_0)$ versus time for the reduction of dyes [(B) methylene blue, (D) methylene orange, and (F) malachite green] in the presence of $NaBH_4$. MB: methylene blue; MO: methylene orange; MG: malachite green.

The zeta potential of produced AgNPs was documented as a highly negative charge (−49 mV), which implies that the AgNPs are more stable by preventing them from aggregation due to electrostatic repulsive force (Suresh et al., 2011). Zeta potential analysis is a technique used to determine the magnitude of the electric charge present on the surface of a given material. The high negative zeta potential value is an effective repellent against particle aggregation or agglomeration. This observation suggests the colloidal stability of the AgNPs. Conversely, nanoparticles possessing a notably reduced negative charge exhibit enhanced cellular penetration capabilities. The observed result indicates that the AgNPs exhibited stability and a uniform distribution. Previous studies like Maillard et al. (2018) have documented the zeta potential values of AgNPs produced from different materials. The results of the DLS documented the mean size of AgNPs as 88.10 nm. The size obtained from the results of the DLS was larger because of the compounds existing in the aqueous extract of *H. tiliaceus* leaf and due to the agglomeration of the synthesized AgNPs. The variation in the AgNPs size range between DLS and HR-TEM might also be because of the water molecules absorbed on electrostatically stabilized AgNPs (Das et al., 2013). The exact size and shape of the produced AgNPs were analyzed using an HR-TEM. Based on the observations from TEM analysis, it can be deduced that the *H. tiliaceus* leaf extract mediated AgNPs exhibited a high degree of uniformity size distribution with characteristic spherical morphology. As seen in the Zeta potential study, AgNPs were not agglomerated in the HR-TEM pictures, which may have been caused by the AgNPs' significant negative charge.

The biosynthesized AgNPs showed potent antioxidant activity in total antioxidant, DPPH, and reducing power assays. In support of our results, Khane et al. (2022) biosynthesized AgNPs from *Citrus limon* Zest extract and showed potential antioxidant activity. Also, Ghatage et al. (2023) synthesized AgNPs from *Aloe barbadensis miller* leaves extract and showed potential antioxidant activity. Moreover, studies have demonstrated that the *H. tiliaceus* L. leaves extract has substantial antioxidant activity because of the redox characteristics of its key natural antioxidants, such as phenolic acids and flavonoids (Surana

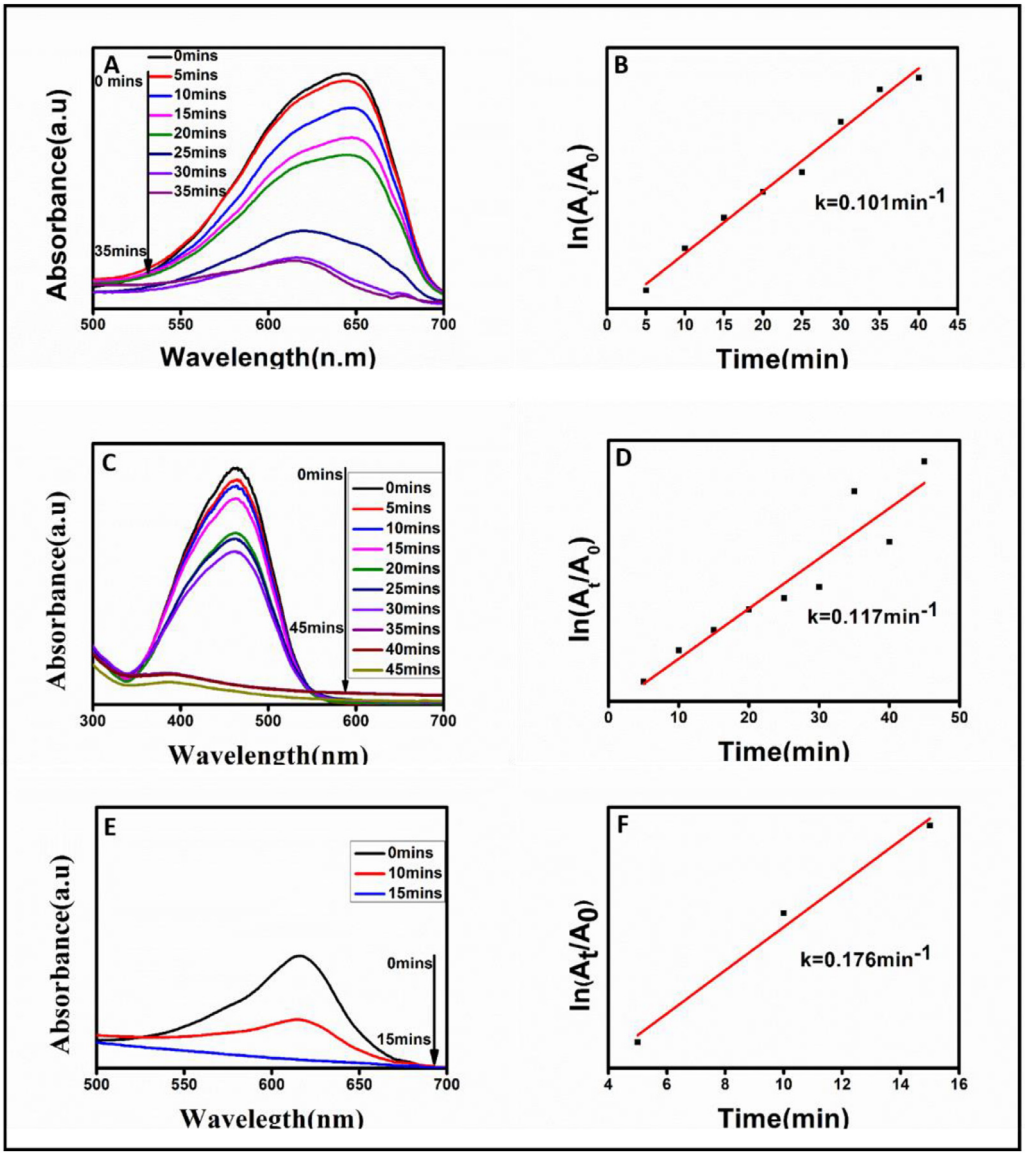

Fig. 6. UV-visible absorption spectra of degradation of dyes [(A) methylene blue, (C) methylene orange, and (E) malachite green] in the presence of $NaBH_4$ and catalyst AgNPs. The plot of $\ln(A_t/A_0)$ versus time for the reduction of dyes [(B) methylene blue, (D) methylene orange, and (F) malachite green] in the presence of $NaBH_4$ and catalyst AgNPs. MB: methylene blue; MO: methylene orange; MG: malachite green.

et al., 2022; Andriani et al., 2020). Thus, the antioxidant capacity of biosynthesized AgNPs may be influenced by the presence of phenolic and flavonoid compounds of *H. tiliaceus* L. leaf extract that coats the AgNPs.

The biosynthesized AgNPs have exhibited broad-spectrum antibacterial activity against Gram-positive and Gram-negative bacteria. In support of our observations, Khane et al. (2022) biosynthesized AgNPs from *C. limon* Zest extract and showed a broad-spectrum antimicrobial activity against Gram-negative and Gram-positive bacteria, as well as fungi. Recently, Ghatage et al. (2023) synthesized AgNPs from *A. barbadensis miller* leaves extract and showed potent antimicrobial activity against both Gram-positive bacteria (*S. aureus* and *S. citrus*) and Gram-negative bacteria (*E. coli* and *K. pneumoniae*). The observed outcomes can be attributed to the AgNPs' initiation of Ag^+ ions. Phospholipid bilayers and protein biomolecules comprise the cell membrane of bacteria, and the phospholipid bilayer is negatively charged. It has been claimed that the oligodynamic effect of silver has antibacterial properties against microbes (Prasher et al., 2018). This is mainly because the surface changes of the particles result in binding affinity towards the bacterial biomolecules, which in turn triggers cell penetration and the generation of reactive oxygen species (ROS), which increases the chemical reactivity of the cells and causes AgNPs to have antibacterial activity. As a result, when positively charged silver ions interact with negatively charged

Table 2
The rate constant (k) and regression values (R^2) and time (mins) for degradation of methylene blue (MB), methyl orange (MO), and malachite green (MG) by catalyst silver nanoparticles (AgNPs) in the presence of reducing agent $NaBH_4$.

Dye degradation	Rate constant (k) min^{-1}	Regression value (R^2)	Time (min)
MB+$NABH_4$	0.029	0.9431	60
MB+$NABH_4$+AgNPs	0.101	0.9884	35
MO+$NABH_4$	0.027	0.9434	60
MO+$NABH_4$+ AgNPs	0.117	0.9230	45
MG+$NABH_4$	0.052	0.8235	60
MG+$NABH_4$+AgNPs	0.176	0.9879	15

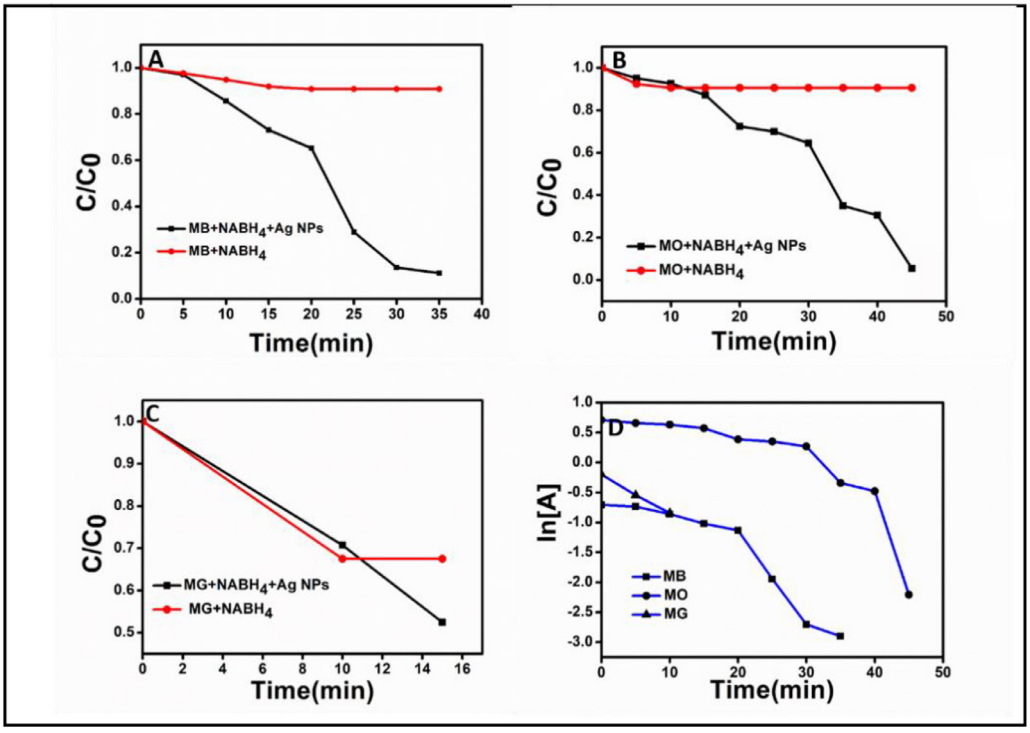

Fig. 7. Dye degradation efficiency of catalyst AgNPs by plots between C/C_o Vs Time for (A) methylene blue, (B) methylene orange, and (C) malachite green. (D) Induction period plot between ln[A] Vs Time for methylene blue, methylene orange, and malachite green. MB: methylene blue; MO: methylene orange; MG: malachite green.

bacterium cell bilayers, the resulting physical alterations to the bacterial species' cell walls cause serious harm (Maillard et al., 2018). Furthermore, research has shown that the strong antimicrobial properties of silver nanoparticles may be related to the fact that their entry into cells damages cell walls, causes porosity, and ultimately results in necrosis (Rautela and Rani, 2019). They also tend to obstruct bacterial growth signaling and facilitate passageways by tempering the tyrosine phosphorylation of presumed peptides substrate essential for cell sustainability and detachment, attacking off the tyrosine kinase enzyme. Additionally, the

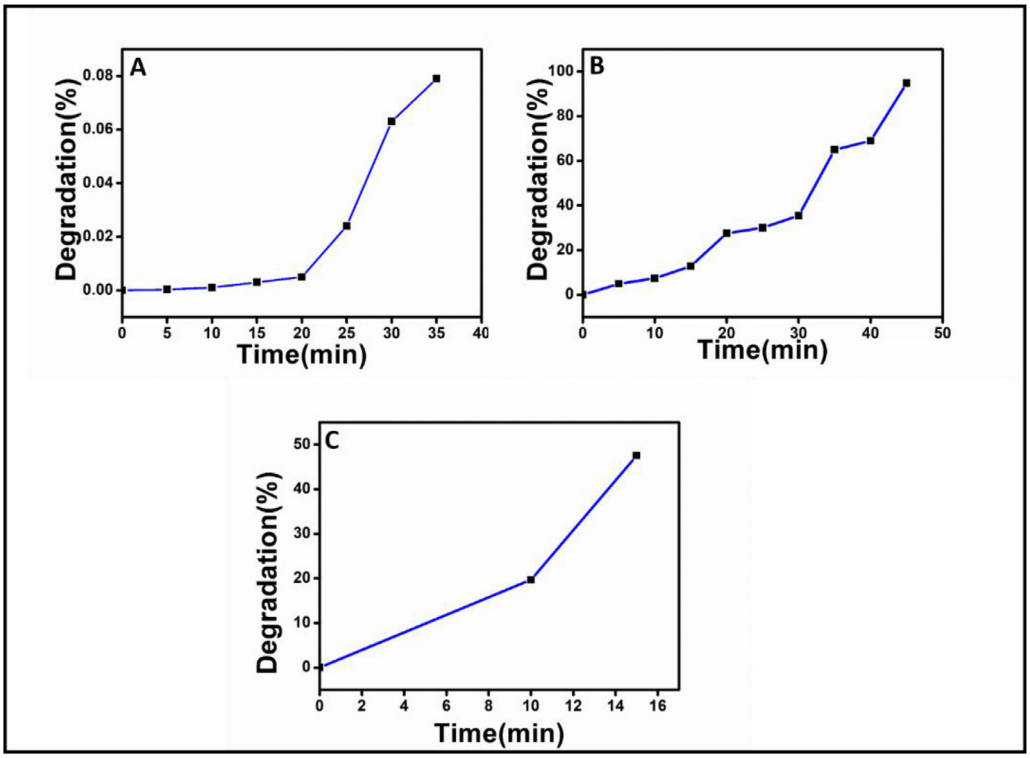

Fig. 8. Percentage of dye degradation of methylene blue, methyl orange, and malachite green by $NaBH_4$ in the presence of catalyst AgNPs. MB: methylene blue; MO: methylene orange; MG: malachite green.

sulfhydryl group (-SH) of the bacterial enzyme may be affected by the silver ions, which could harm the enzymes (Hovhannisyan et al., 2022; Scandorieiro et al., 2022).

Most chronic diseases like cardiovascular diseases and cancer are due to oxidative stress, which is the leading root cause. (Shimada et al., 1992). The protective character of antioxidants against oxidative-stress-connected disorders has been confirmed (Sies et al., 1997). Bio-products like plants have antioxidant properties that exhibit growth-suppression and apoptosis properties of cancerous cells, which might be appropriate for treating cancer with no side effects. Plant-related treatments employing the green synthesized AgNPs have also exhibited enhanced anti-cancer properties (Sathelly et al., 2022). Henceforth, in our present research, we have evaluated the anticancer property of AgNPs synthesized using *H. tiliaceus* aqueous leaf extract. Under *in-vitro* conditions, the synthesized AgNPs have shown potential anticancer activity against the human breast cancer cell line MCF-7. In support of our study, several researchers have proven the excellent anticancer activity of green synthesized AgNPs (Ghatage et al., 2023; Andriani et al., 2020; He et al., 2017; Naraginti and Li, 2017; Mukundan et al., 2015). The researchers pointed out that the synergy between AgNPs and the covering polyphenols of the leaf extract is the primary reason for the elevated anticancer activity of the AgNPs. Moreover, increased uptake of nanoparticles by these cancer cells causes the greater anticancer effect of AgNPs. Cancerous cells are highly vulnerable because of the high proliferation rate and irregular metabolism (Cairns et al., 2011). The synchronized effect of AgNPs and polyphenols increases ROS production and constrains the transcription process. Notably, cytotoxicity is displayed by antioxidants such as polyphenols only against abnormal cells (Li et al., 2006). The data in the literature support the statement, which reported the concentration-dependent cytotoxicity of nanoparticles, particularly at a lower level (Park et al., 2010; Palaniappan et al., 2015).

The produced AgNPs were used as a catalyst in the methylene blue (MB), methylene orange (MO), and malachite green (MG) dye degradation processes. When dye degradation was attempted solely using $NaBH_4$ as a reducing agent, MB, MO, and MG did not degrade successfully because there was insufficient electron transfer between the dye (the acceptor) and $NaBH_4$ (the donor) due to the high bond dissociation energy (BDE). In the mixture used for the reaction between dyes and $NaBH_4$ ions, the AgNPs nanocatalyst is introduced as an intermediary. In addition to lowering BDE and demonstrating that the rate of MB, MO, and MG reduction by $NaBH_4$ was accelerated in the presence of AgNPs, it was observed in this experiment that the dye degraded quickly (Moond et al., 2023). In support of our report, several researchers green synthesized AgNPs and reported as a perfect catalyst for dye degradation (Ghatage et al., 2023; Naraginti and Li, 2017; Bhakya et al., 2015; Mata et al., 2015).

The color of the dyes is due to their absorbance of light in the visible spectrum 350–700 nm. For any dye, there will be at least one color-imparting group known as a chromophore, for example, nitro, azo, anthraquinone moiety, phthalocyanine, methine group, etc., and color enriching groups, which also influence their solubility known as auxo chromes, like COOH, SO_3H or OH groups. The dye loses its color if any of these characters (chromophore, auxo chromes) are affected or lost from the molecular structures of the dye by breaking their structural bonds; there are several agents to this since chemical reactions are involved in breaking old bonds and the creation of new bonds. As per bond dissociation energy (BDE) theory, the lower the BDE is, the more powerful the chemical bond is and the easier it is for old bonds to break and new bonds to form. It is well known that an aqueous solution of sodium borohydride liberates hydrogen by forming sodium borohydroxide in the presence of a catalyst (Xu et al., 2008). The liberated hydrogen helps in the reduction of the dye.

The reaction between the reducing agent $NaBH_4$ and the dye is due to the electron transfer reaction where $NaBH_4$ donates the electrons and the test dye to be degraded receives the electron (Pal et al., 1998). When nanoparticles are added as nanocatalysts, they act as a potential barrier between the BH_4^- ions and the dye and facilitate faster electron transfer during redox reactions. The surface area of the nanoparticles is responsible for an increase in the transfer rate of electrons and enhances the degradation process. Before the transfer of electrons, both the $NaBH_4$ and the dye attach to the nanoparticles' surface. The phytochemical molecules in the nanoparticles help this course by getting them to the surface of the nanoparticles by the electrostatic force of interaction. Afterward, the BH_4^- ions release the electrons on the surface of the nanoparticles, thereby transferring them to the dye and facilitating dye degradation. This accounts for the nanoparticles as nanocatalysts in increasing the reaction rate in dye degradation processes.

5. Conclusion

Eco-friendly AgNPs were successfully prepared from *H. tiliaceus* leaf aqueous extract as a reducing and stabilizing agent. The confirmation of synthesized AgNPs was revealed by a UV-visible spectrophotometer, which showed confirmatory absorbance at 420 nm. FTIR concluded that the phytochemical compounds of *H. tiliaceus* leaf aqueous extract facilitated the synthesis of eco-friendly AgNPs. Further nanotechnology studies confirmed that AgNPs were nano in size and have stability. The synthesized AgNPs were shown to have potential biological activities such as antibacterial, antioxidant, and anticancer activities. Further, AgNPs showed dye degradation activity and were found to be highly applicable to environmental remediation. The study concluded that synthesized AgNPs have excellent nanotechnology features and biological applications and could be highly useful in biomedical and environmental fields. However, toxicity and safety issues of AgNPs should be considered for further assurance.

Declaration of competing interest

The authors declare that they have no known competing financial interests or personal relationships that could have appeared to influence the work reported in this paper.

CRediT authorship contribution statement

Vinay Viswanath Konduri: Conceptualization, Data curation, Formal analysis, Investigation, Visualization, Writing – original draft. **Naveen Kumar Kalagatur:** Investigation, Visualization, Writing – original draft. **Lokanadhan Gunti:** Data curation, Formal analysis, Writing – original draft. **Usha Kiranmayi Mangamuri:** Conceptualization, Data curation, Formal analysis, Investigation, Visualization, Writing – original draft. **Venkateswara Rao Kalagadda:** Conceptualization, Data curation, Formal analysis, Investigation, Visualization, Writing – original draft. **Sudhakar Poda:** Conceptualization, Data curation, Project administration, Formal analysis, Investigation, Visualization, Writing – original draft. **Suresh Babu Naidu Krishna:** Data curation, Resources, Formal analysis, Validation, Writing – review & editing.

Acknowledgment

The authors thanked Acharya Nagarjuna University, India, for providing the facilities. KSBN would like to thank Durban University of Technology (DUT) for the research fellowship and Director, IWWT, DUT.

References

Abdul-Awal, S.M., Nazmir, S., Nasrin, S., Nurunnabi, T.R., Uddin, S.J., 2016. Evaluation of the pharmacological activity of *Hibiscus tiliaceus*. Springerplus 5 (1), 1–6.

Ajitha, B., Reddy, Y.A.K., Reddy, P.S., 2014. Biogenic nano-scale silver particles by *Tephrosia purpurea* leaf extract and their inborn antimicrobial activity. Spectrochim. Acta A Mol. Biomol. Spectrosc. 121, 164–172.

Andriani, Y., Sababathy, M., Amir, H., Sarjono, P.R., Syamsumir, D.F., Sugiwati, S., Kassim, M.N.I., 2020. The potency of *Hibiscus tiliaceus* leaves as antioxidant and anticancer agents via induction of apoptosis against MCF-7 cells. IOP Conf. Ser. Mater. Sci. Eng. 959, 012022.

Bar, H., Bhui, D.K., Sahoo, G.P., Sarkar, P., De, S.P., Misra, A., 2009. Green synthesis of silver nanoparticles using latex of *Jatropha curcas*. Colloids Surf. A Physicochem. Eng. 339, 134–139.

Bhakya, S., Muthukrishnan, S., Sukumaran, M., Muthukumar, M., Kumar, S.T., Rao, M.V., 2015. Catalytic degradation of organic dyes using synthesized silver nanoparticles: a green approach. Int. J. Environ. Bioremediat. Biodegrad. 6 (5), 1.

Cairns, R.A., Harris, I.S., Mak, T.W., 2011. Regulation of cancer cell metabolism. Nat. Rev. Cancer 11 (2), 85–95.

Das, S., Roy, P., Mondal, S., Bera, T., Mukherjee, A., 2013. One pot synthesis of gold nanoparticles and application in chemotherapy of wild and resistant type visceral leishmaniasis. Colloids Surf. B 107, 27–34.

Ghatage, M.M., Mane, P.A., Gambhir, R.P., Parkhe, V.S., Kamble, P.A., Lokhande, C.D., Tiwari, A.P., 2023. Green synthesis of silver nanoparticles via *Aloe barbadensis miller* leaves: anticancer, antioxidative, antimicrobial and photocatalytic properties. Appl. Surf. Sci. Adv. 16, 100426.

González-Palma, I., Escalona-Buendía, H.B., Ponce-Alquicira, E., Téllez-Téllez, M., Gupta, V.K., Díaz-Godínez, G., Soriano-Santos, J., 2016. Evaluation of the antioxidant activity of aqueous and methanol extracts of *Pleurotus ostreatus* in different growth stages. Front Microbiol. 7, 1099.

Gunti, L., Dass, R.S., Kalagatur, N.K., 2019. Phytofabrication of selenium nanoparticles from *Emblica officinalis* fruit extract and exploring its biopotential applications: antioxidant, antimicrobial, and biocompatibility. Front Microbiol 10, 931.

Gunti, L., Dass, R.S., Mahata, P.K., 2022. Multifaceted role of phyto-assisted selenium nanoparticles (SeNPs) in biomedical and human therapeutics. Selenium and Nano-Selenium in Environmental Stress Management and Crop Quality Improvement. Springer, Cham, pp. 437–458.

He, Y., Wei, F., Ma, Z., Zhang, H., Yang, Q., Yao, B., Huang, Z., Li, J., Zeng, C., Zhang, Q., 2017. Green synthesis of silver nanoparticles using seed extract of *Alpinia katsumadai*, and their antioxidant, cytotoxicity, and antibacterial activities. RSC Adv. 7 (63), 39842–39851.

Hovhannisyan, Z., Timotina, M., Manoyan, J., Gabrielyan, L., Petrosyan, M., Kusznierewicz, B., Bartoszek, A., Jacob, C., Ginovyan, M., Trchounian, K., Sahakyan, N., Nasim, M.J., 2022. *Ribes nigrum* L. Extract-mediated green synthesis and antibacterial action mechanisms of silver nanoparticles. Antibiotics 11 (10), 1415.

Jeeva, K., Thiyagarajan, M., Elangovan, V., Geetha, N., Venkatachalam, P., 2014. *Caesalpinia coriaria* leaf extracts mediated biosynthesis of metallic silver nanoparticles and their antibacterial activity against clinically isolated pathogens. Ind. Crops Prod 52, 714–720.

Joseph, S., Mathew, B., 2015. Facile synthesis of silver nanoparticles and their application in dye degradation. Mater. Sci. Eng. B 195, 90–97.

Kalagatur, N.K., Gurunathan, S., Kamasani, J.R., Gunti, L., Kadirvelu, K., Mohan, C.D., Rangappa, S., Prasad, R., Almeida, F., Mudili, V., Siddaiah, C., 2020. Inhibitory effect of *C. zeylanicum, C. longa, O. basilicum, Z. officinale*, and *C. martini* essential oils on growth and ochratoxin A content of *A. ochraceous* and *P. verrucosum* in maize grains. Biotechnol. Rep. 27, e00490.

Kalagatur, N.K., Kamasani, J.R., Mudili, V., 2018. Assessment of detoxification efficacy of irradiation on zearalenone mycotoxin in various fruit juices by response surface methodology and elucidation of its *in-vitro* toxicity. Front. Microbiol. 9, 2937.

Kalagatur, N.K., Karthick, K., Allen, J.A., Nirmal Ghosh, O.S., Chandranayaka, S., Gupta, V.K., Krishna, K., Mudili, V., 2017. Application of activated carbon derived from seed shells of *Jatropha curcas* for decontamination of zearalenone mycotoxin. Front. Pharmacol. 8, 760.

Khane, Y., Benouis, K., Albukhaty, S., Sulaiman, G.M., Abomughaid, M.M., Al Ali, A., Aouf, D., Fenniche, F., Khane, S., Chaibi, W., Henni, A., Bouras, H.D., Dizge, N., 2022. Green synthesis of silver nanoparticles using aqueous *Citrus limon* zest extract: characterization and evaluation of their antioxidant and antimicrobial properties. Nanomaterials 12 (12), 2013.

Lakshmeesha, T.R., Kalagatur, N.K., Mudili, V., Mohan, C.D., Rangappa, S., Prasad, B.D., Ashwini, B.S., Hashem, A., Alqarawi, A.A., Malik, J.H., Abd_Allah, E.F., Gupta, V.K., Siddaiah, C.N., Niranjana, S.R., 2019. Biofabrication of zinc oxide nanoparticles with *Syzygium aromaticum* flower buds extract and finding its novel application in controlling the growth and mycotoxins of *Fusarium graminearum*. Front. Microbiol. 10, 1244.

Li, L., Tsao, R., Yang, R., Liu, C., Zhu, H., Young, J.C., 2006. Polyphenolic profiles and antioxidant activities of heartnut (Juglans ailanthifolia var. cordiformis) and Persian walnut (Juglans regia L.). J. Agric. Food Chem. 54 (21), 8033–8040.

Lim, W.Y., Chan, E.W.C., Phan, C.W., Wong, C.W., 2022. Emulsion formulated using *Hibiscus tiliaceus* L. extract and flaxseed oil for topical application. Ind. Crops Prod. 188, 115718.

Maillard, A.P.F., Dalmasso, P.R., de Mishima, B.A.L., Hollmann, A., 2018. Interaction of green silver nanoparticles with model membranes: possible role in the antibacterial activity. Colloids Surf. B 171, 320–326.

Maheswari, J., Reshma Anjum, M., Sankari, M., Narasimha, G., Krishna, S.B.N., Kishori, B., 2023. Green synthesis, characterization and biological activities of silver nanoparticles synthesized from *Neolamarkia cadamba*. ADMET DMPK 11, 573–585.

Mata, R., Nakkala, J.R., Sadras, S.R., 2015. Catalytic and biological activities of green silver nanoparticles synthesized from *Plumeria alba* (frangipani) flower extract. Mater. Sci. Eng. C 51, 216–225.

Moond, M., Singh, S., Sangwan, S., Devi, P., Beniwal, A., Rani, J., Kumari, A., Rani, S., 2023. Biosynthesis of silver nanoparticles utilizing leaf extract of Trigonella foenum-graecum L. for catalytic dyes degradation and colorimetric sensing of Fe3 +/Hg2+. Molecules 28 (3), 951.

Mukundan, D., Mohankumar, R., Vasanthakumari, R., 2015. Green synthesis of silver nanoparticles using leaves extract of *Bauhinia tomentosa* linn and its *in vitro* anticancer potential. Mater. Today Proc. 2 (9), 4309–4316.

Muniyandi, K., George, E., Mudili, V., Kalagatur, N.K., Anthuvan, A.J., Krishna, K., Thangaraj, P., Natarajan, G., 2017. Antioxidant and anticancer activities of *Plectranthus stocksii* Hook. f. leaf and stem extracts. Agric Nat Resour 51 (2), 63–73.

Naraginti, S., Kumari, P.L., Das, R.K., Sivakumar, A., Patil, S.H., Andhalkar, V.V., 2016. Amelioration of excision wounds by topical application of green synthesized, formulated silver and gold nanoparticles in albino Wistar rats. Mater. Sci. Eng. C 62, 293–300.

Naraginti, S., Li, Y., 2017. Preliminary investigation of catalytic, antioxidant, anticancer and bactericidal activity of green synthesized silver and gold nanoparticles using *Actinidia deliciosa*. J. Photochem. Photobiol. B 170, 225–234.

Narayanan, K.B., Sakthivel, N., 2011. Green synthesis of biogenic metal nanoparticles by terrestrial and aquatic phototrophic and heterotrophic eukaryotes and biocompatible agents. Adv. Colloid Interface Sci. 169 (2), 59–79.

Palaniappan, P., Sathishkumar, G., Sankar, R., 2015. Fabrication of nano-silver particles using *Cymodocea serrulata* and its cytotoxicity effect against human lung cancer A549 cells line. Spectrochim. Acta A Mol. Biomol. 138, 885–890.

Park, E.J., Yi, J., Kim, Y., Choi, K., Park, K., 2010. Silver nanoparticles induce cytotoxicity by a Trojan-horse type mechanism. Toxicol. *In Vitro* 24 (3), 872–878.

Prasher, P., Singh, M., Mudila, H., 2018. Oligodynamic effect of silver nanoparticles: a review. BioNanoSci 8, 951–962.

Prieto, P., Pineda, M., Aguilar, M., 1999. Spectrophotometric quantitation of antioxidant capacity through the formation of a phosphomolybdenum complex: specific application to the determination of vitamin E. Anal. Biochem. 269 (2), 337–341.

Raj, C.D., Muthukumar, K., Dahms, H.U., James, R.A., Kandaswamy, S., 2023. Structural characterization, antioxidant and anti-uropathogenic potential of biogenic silver nanoparticles using brown seaweed *Turbinaria ornata*. Front. Microbiol 14, 1072043.

Rautela, A., Rani, J., 2019. Green synthesis of silver nanoparticles from *Tectona grandis* seeds extract: characterization and mechanism of antimicrobial action on different microorganisms. J. Anal. Sci. Technol. 10 (1), 1–10.

Rosaiah, G., Mangamuri, U.K., Sikharam, A.S., Devaraj, K., Kalagatur, N.K., Kadirvelu, K., 2022. Biosynthesis of selenium nanoparticles from *Annona muricata* fruit aqueous extract and investigation of their antioxidant and antimicrobial potentials. Curr. Trends Biotechnol. Pharm. 16 (1), 101–107.

Sathelly, K., Kalagatur, N.K., Mangamuri, U.K., Puli, C.O.R., Poda, S., 2022. Anticancer potential of *Solanum lycopersicum* L. extract in human lung epithelial cancer cells A549. Indian J. Biochem. Biophys. 60 (1), 76–85.

Scandorieiro, S., Rodrigues, B.C., Nishio, E.K., Panagio, L.A., De Oliveira, A.G., Durán, N., Nakazato, G., Kobayashi, R.K., 2022. Biogenic silver nanoparticles strategically combined with *Origanum vulgare* derivatives: antibacterial mechanism of action and effect on multidrug-resistant strains. Front. Microbiol. 13, 842600.

Shimada, K., Fujikawa, K., Yahara, K., Nakamura, T., 1992. Antioxidative properties of xanthan on the autoxidation of soybean oil in cyclodextrin emulsion. J. Agric. Food Chem. 40 (6), 945–948.

Sies, H., 1997. Oxidative stress: oxidants and antioxidants. Exp. Physiol. 82 (2), 291–295.

Suba, S., Vijayakumar, S., Nilavukkarasi, M., Vidhya, E., Punitha, V.N., 2022. Eco synthesized silver nanoparticles as a next generation of nanoproduct in multidisciplinary applications. J. Environ. Chem. Ecotoxicol. 4, 13–19.

Surana, A.R., Kumbhare, M.R., Gunjal, A.R., Goswami, S.S., Ghuge, D.M., 2022. Chemical characterization, thrombolytic and antioxidant activity of *Hibiscus tiliaceus* L. leaves. Nat. Prod. Res. 36 (23), 6106–6110.

III Suresh, A.K., Doktycz, M.J., Wang, W., Moon, J.W., Gu, B., Meyer, H.M., Hensley, D.K., Allison, D.P., Phelps, T.J., Pelletier, D.A., 2011. Monodispersed biocompatible silver sulfide nanoparticles: facile extracellular biosynthesis using the γ-proteobacterium, *Shewanella oneidensis*. Acta Biomater. 7 (12), 4253–4258.

Swaminathan, S., Haribabu, J., Kalagatur, N.K., Konakanchi, R., Balakrishnan, N., Bhuvanesh, N., Karvembu, R., 2019. Synthesis and anticancer activity of [RuCl2 (η6-arene)(aroylthiourea)] complexes—High activity against the human neuroblastoma (IMR-32) cancer cell line. ACS Omega 4 (4), 6245–6256.

Vundela, S.R., Kalagatur, N.K., Nagaraj, A., Kadirvelu, K., Chandranayaka, S., Kondapalli, K., Hashem, A., Abd_Allah, E.F., Poda, S., 2022. Multi-biofunctional properties of phytofabricated selenium nanoparticles from *Carica papaya* fruit extract: antioxidant, antimicrobial, antimycotoxin, anticancer, and biocompatibility. Front. Microbiol. 12, 769891.

Xu, L., Wu, X.C., Zhu, J.J., 2008. Green preparation and catalytic application of Pd nanoparticles. Nanotechnology 19, 305603.